Removal of Methylene Blue from aqueous solution by Fe_3O_4@Ag/SiO_2 nanospheres: Synthesis, characterization and adsorption performance

Jyoti Saini[a], V. K. Garg[b], R. K. Gupta[a]

[a]*Department of Chemistry, Guru Jambheshwar University of Science and Technology, Hisar 125001, Haryana, India,*

[b]*Centre for Environmental Sciences and Technology, School of Environment and Earth Sciences, Central University of Punjab, Bathinda - 155001, Punjab, India,*

Abstract

In this study, silver silica coated magnetite (Fe_3O_4@Ag/SiO_2)nanospheres were synthesized via sonication method and their performance was evaluated as nanoadsorbents for removal of Methylene Blue in batch mode experiments. The physical characteristics of these nanospheres were studied using XRD, SEM, EDX, TEM, and FTIR techniques. The Fe_3O_4@Ag/SiO_2 nanospheres were able to achieve 99.6% removal of Methylene Blue at pH 7. A possible mechanism for adsorption of Methylene Blue onto Fe_3O_4@Ag/SiO_2 has been proposed. The adsorption equilibrium and kinetics were studied for experimental data of Methylene Blue. The removal process agreed well with Langmuir isotherm model with maximum monolayer adsorption capacity 128.5 mg/g. Experimental kinetic data fitted well with the Pseudo-second-order and Intraparticle diffusion model. The analysis of thermodynamic parameters ΔG^0, ΔS^0 and ΔH^0 proposed spontaneous, endothermic and feasible adsorption of Methylene Blue under investigated experimental conditions. The Fe_3O_4@Ag/SiO_2 nanospheres were regenerated and reusable for five successive cycles.

Keywords: Dye removal, silver silica coated magnetite nanospheres (Fe_3O_4@Ag/SiO_2), SEM, Kinetics, Equilibrium adsorption isotherm, Methylene Blue (MB)

1 Introduction

Water pollution is a global problem. Major colour contributors in wastewater are residual dyes generated from textiles, paper mills and dyeing industries at large scale. The residual dye solution contains non-biodegradable toxic organic pollutants which interrupt photosynthetic activity in aquatic system and retards growth of the biotic community [1, 2]. Spent dyes in the aqueous stream make water unsuitable for consumption. Methylene Blue (MB) is being used for dyeing cotton, wool, silk, leather, and paper, also in cosmetics, pharmaceuticals, tannery and food processing industries. Hence its amalgamation in aquatic stream causes harmful effects such as; eye irritation in human as well as animals, irritates the gastrointestinal tract along with vomiting, diarrhea and nausea [37, 34].

Now day's transition metals and their oxides had been widely used in wastewater treatment via adsorption process. Among them magnetite (Fe_3O_4) nanoparticles have attracted much attention not only in water decontamination, but also in the fields like drug delivery system, magnetic resonance imaging and magnetic sensing etc. [4]. Bare magnetite nanoparticles are highly susceptible to air oxidation and leaching under acidic conditions. Therefore a surface modification is necessary to enhance the stability and potential of magnetite nanoparticles in various fields [5-7]. Recently silica coating is considered as promising surface modifier due to its thermal stability, nontoxicity, resistant to acid and alkali, uniform size and shape. Silica coating not only protects the inner magnetite core from oxidation, but also presence of various functional groups enhances the adsorption capacity of the magnetite nanomaterials [6-9]. Recently, a few synthesized adsorbents for removal of MB are;phytic acid modified $CoFe_2O_4$ magnetic adsorbent with controllable morphology, mixed titanium, silicon, and aluminum oxide nanostructures, cross-linked beads of activated oil palm ashzeolite/Chitosan composite as a bio-adsorbent, sulfuric acid–treated orange peel, Ni-metal organic framework and many more. Still, some more efficient and economic adsorbents are needed. [37,3 9-11].

The present study reports the synthesis and characterization of silver silica coated magnetitenanospheres (Fe_3O_4@Ag/SiO_2) and their usability as nanoadsorbents for the removal of Methylene Blue dye from simulated solution under various process conditions.

2 EXPERIMENTAL SECTION

2.1 Reagents and Materials

All the solutions were prepared in double distilled water. The reagents in experimental study were of analytical grade and used without further purification. Ferric chloride hexahydrate, ferrous chloride, tetraethoxysilane, silver nitrate, ethanol and ammonia solution were purchased from Himedia Laboratory Pvt. Ltd., India. Methylene Blue was procured from SD fine-Chem Ltd, Mumbai. The physico-chemical properties of MB dye are given in Table 1.

2.2 Synthesis and Preparation of the adsorbent

Preparation of Fe_3O_4 nanospheres

Sonication method was used to prepare bare Fe_3O_4 nanoparticles [12]. 0.02 mole of $FeCl_3.6H_2O$ and 0.01mole of $FeCl_2.4H_2O$ were dissolved in 100 ml of distilled water. Subsequently liquid ammonia was added drop wise to the above solution for 30 min. under constant magnetic stirring. Then, the mixture was transferred to the sonicator for 1h. Black precipitates were formed and separated by centrifugation pump. The obtained Fe_3O_4 nanospheres were washed twice with deionised water and ethanol, and then dried in oven at 100 for 6h.

Preparation of Ag/SiO_2 nanoparticles

Ag/SiO_2 nanoparticles were prepared by modifying the Stobber method [13]. 0.01 M $AgNO_3$ was added to absolute ethanol-water 2:1 (v/v) mixture under sonication bath. Then 20 ml of liquor ammonia was dropped slowly into the reaction mixture in the ultrasonic bath After that, 5 ml tetraethoxysilane was added to the above mixture

following sonication for 2 h. The obtained white gel was centrifuged, washed with deionised water and dried in oven at 100˚C for 2h. Finally fine white nanopowder of Ag/SiO_2 was obtained.

Preparation of Fe_3O_4@Ag/SiO_2 nanoparticles

1.5 g prepared Fe_3O_4 nanoparticles were dissolved in ethanol-water (1:1) mixture with continuous magnetic stirring at room temperature. Then 3.0 g of already produced Ag/SiO_2nanoparticles were dispersed in the above reaction mixture. The suspension was stirred for 15 minutes and finally transferred to sonication bath for 4 h. The colour of the suspension changes creams to brownish. The product was collected by centrifugation, washed and calcined at 80˚C. Finally fabricated Fe_3O_4@Ag/SiO_2 nanospheres were obtained. The possible interactions of Fe_3O_4 nanospheres with Ag/SiO_2 nanospheres are given in scheme 1.

2.3 Characterization of nanospheres

The crystal structure of Ag/SiO_2, Fe_3O_4 and Fe_3O_4@Ag/SiO_2 was investigated using X-ray diffraction (XRD). XRD patterns of the samples were analyzed at room temperature using a Rigaku Miniflex-II diffractometer with Cu Ka radiation in the 2 θ range ($20\text{-}80^0$) at a scanning rate of 2^0/min. The IR spectrum of samples was recorded on SHIMADIZU IR AFFINITY-I FTIR spectrophotometer using KBr powder. The surface morphology, textural structure and elemental constituents of samples were obtained by scanning electron microscope (SEM) and energy-dispersive X-ray spectroscopy (EDX) using Merlin Compact 6073 Scanning Electron Microscope (Carl Zeiss, Germany). Transmission electron microscopy was done to determine the particle size of Fe_3O_4@Ag/SiO_2 by Morgagni 268D (Fei Electron Optics, AIIMS India).

Concentration of MB dye was determined by UV-VIS spectrophotometer at (LABINDIA, Model UV-VIS 3000^+) 664 nm.

2.4 Adsorption Experiments

All the batch mode experiments were conducted by agitating optimal amount of adsorbent dose in 50mL of dye solution of desired concentration, pH, contact time and solution temperature in a thermostat covered shaker at 120 rpm.The influence of pH on adsorption of MB dye was analyzed over the pH range of 2-10. The pH was adjusted using 0.1 mol/L NaOH or HCl solution. The effect of adsorbent mass on the removal of MB was studied in the range of (0.01-0.1g) per 50mL dye of 50mg/L at pH 7 for 50 min. Batch equilibrium adsorption experiments were carried out by contacting 50mL of 50mg/L MB solution with 0.03g of adsorbent for 50 min. at room temperature and of pH 7. Thermodynamic studies were conducted at a temperature range of (10˚-50˚C) keeping all the parameters same as given above. The samples were agitated and withdrawn from the shaker at predetermined time intervals. Adsorbent was separated from the dye solution by centrifugation technique. Absorbance and concentration of the obtained supernatant were measured by UV-visible spectrophotometer. The removal percentage and adsorption capacity of the residual MB solution were determined by the following equations;

$$Dye\ removal\ (\%) = \frac{(C_o - C_e)}{C_o} \times 100 \quad (1)$$

$$Adsorption\ capacity\ (q_e) = \frac{(C_o - C_e)\,V}{m} \quad (2)$$

where C_0 (mg/L) and C_e (mg/L) are the initial and equilibrium concentration of dye solution, q_e (mg/g) denote the amount of MB adsorbed onto the adsorbent, V is the volume of solution (L) and m is the mass of adsorbent (g).

3 Results and Discussion

3.1 Characterization of adsorbents

Fe_3O_4@Ag/SiO_2 nanoparticles were characterized by FTIR XRD, SEM, EDX and TEM as described below:

The surface group functionalization and binding sites of Fe_3O_4@Ag/SiO_2 were identified by FTIR spectrum (Fig. 1a-c). Strong doublet peaks in Fig.1a at 620-650 cm^{-1} corresponds to the stretching vibrations of Fe-O bond in Fe_3O_4. Same absorption peak is slightly shifted and appear as a single peak in Fe_3O_4@Ag/SiO_2 indicates participation of Fe-O bond. Sharp peaks at ~493 $cm^{-1}$are associated with Si-O-Si bending vibrations (Fig. 1bc). Another characteristic peak at 783 cm^{-1} may be attributed to symmetric stretching vibrations of of Si–O–Si bonds. Another characteristic signal at 993 cm^{-1} was attributed to Si-O bending vibrations. A strong absorption band at 1093 cm^{-1} is relevant to asymmetric stretching of Si–O–Si bonds. The sharp peak at 1126.36 cm^{-1} is attributed to stretching vibrations of Fe-O-Si bond [5, 6]. The absorption peaks at 1288.6 cm^{-1} and 1537.9 cm^{-1} indicates the formation of Ag nanoparticles [40].The broad absorption band in the range 2800-3700 cm^{-1} was assigned to surface Si-OH groups (Fig. 1bc). Almost similar peaks are seen in the FTIR spectrum of both Ag/SiO_2 and Fe_3O_4@Ag/SiO_2. However, peak intensities of Fe_3O_4@Ag/SiO_2 are deducted, which clearly suggest blending of Fe_3O_4 onto Ag/SiO_2 surface.

To analyze crystalline phase of prepared silver silica coated magnetite (Fe_3O_4@Ag/SiO_2) nanospheres, XRD patterns of Ag/SiO_2, Fe_3O_4 and Fe_3O_4@Ag/SiO_2 were recorded (Fig. 2a-c). The broadband at 2θ =15-20˚is attributed to amorphous silica in Fig. 2a. The diffraction peaks observed at 2θ =30.8°, 34.6°,44.4°, 53.8°, 57.2° 62.7° and 75.2° corresponds to diffraction planes (220), (311), (400), (422), (511), (440) and (533) respectively (Fig. 2b). These observations are in good agreement with previous findings [5-7]. In Fig. 2c, a less intense broadband of silica indicates the incorporation of Fe3O4nanoparticles within the silica surface. Diffraction peaks at 2θ =38. 8° and 64.5° are related to (111) and (220) miller indices of Ag metal. Further, reminder diffraction peaks are found to be broadened as compared to the XRD pattern of Fe_3O_4 suggesting reduction in crystallinity of pristine Fe_3O_4 in Fe_3O_4@Ag/SiO_2. Sharpness and intensity of

peaks are declined in Fe_3O_4@Ag/SiO_2 as compared to pristine Fe_3O_4. It may be due to either incorporation of Fe_3O_4 nanoparticles onto silver silica surface or amorphous nature of silica.

SEM has been used to identify the surface texture and porosity of synthesized Fe_3O_4@Ag/SiO_2 nanoparticles. SEM images of fresh and spent Fe_3O_4@Ag/SiO_2 are shown in Fig. 3a-d. Surface images of unused Ag/SiO_2, Fe_3O_4 andFe_3O_4@Ag/SiO_2 clearly show well defined aggregate spherical nanospheres. Because of strong vander waals and magnetic interactions among Fe_3O_4@Ag/SiO_2, of course aggromolation and anisotropic distribution of nanospheres is observed [39]. Aggregate spheres are observed on the surface of unused nanoparticles i.e. Fe_3O_4@Ag/SiO_2. After adsorption, puffy seeds were seen onto the exhausted materials, which indicate the covering by dye molecules on the surface of Fe_3O_4@Ag/SiO_2 (Fig. 3dd_1). However, fine spherical shape of nanospheres remains same before and after adsorption.

Fig. 4a-d) shows TEM analysis of Fe_3O_4@Ag/SiO_2 nanospheres. These images revealed that Fe_3O_4 nanospheres entrapped successfully into the Ag/SiO_2 shells. The spherical shapes of nanospheres are also confirmed. The average particle size of Fe_3O_4@Ag/SiO_2 nanospheres is about 200 nm as shown in TEM images. EDX analysis has been done to find out the elemental composition of Fe_3O_4@Ag/SiO_2 shown in Fig. 4. The weight percent of the detected elements were Si 19.60, O 35.85, Fe 8.21, and Ag 36.34. No additional energy peak of any other metal was observed.

3.2 Adsorption Experiment

3.2.1 Effect of pH

Fig. 5a shows the dependence of MB adsorption on the pH of the solution. Rapid increase (68.9%-99.2%) in MB removal was observed in the pH range of 2-7. After that adsorption is almost constant up to pH 10. Similar observations have been reported for

adsorption of MB by other authors (Md. Tamez Uddin et al [14] and Flavio Andre Pavan et al [15]). These results may be attributed to electrostatic interactions between adsorbent and adsorbate. Methylene blue is a cationic dye; hence its degree of adsorption is influenced by altering pH of the dye solution and net surface charge on the adsorbent. At lower pH, H^+ ions compete with cationic dye for occupying adsorption sites which results lesser adsorption. However opposite results were obtained at higher pH. These electrostatic interactions are given in scheme 1.

3.2.2 Effect of adsorbent dose

The influence of adsorbent dose on removal of MB was studied in the range of (0.01g-0.1g). The results are shown in Fig. 5b. The results indicate that with the increase in adsorbent dose, the removal percentage of MB increased from 63.2%-98.9%. This may be due to increase in surface area and, consequently, more active sites with enhanced adsorbent concentration. The removal of MB was increased sharply up to 0.03 g adsorbent dose. Further, there was no significant change observed with increasing adsorbent concentration. The increase in removal efficiency was 98.2 % to 98.9% with the adsorbent dose 0.03-0.1g. These results for MB adsorption are in agreement with the findings of other authors [16, 17].

3.2.3 Effect of contact time with dye concentration

The effect of contact time with dye concentration on to dye removal is given in Fig 6a. The removal efficiency of MB was increased from 98.2 %-98.9% within 60 min. The adsorption equilibrium reached in less than 20 min after that there was a negligible change in dye removal of MB. With the passage of time, more active sites of the adsorbent are occupied by the adsorbate. Hence removal efficiency attains equilibrium at certain interval of time. The dye removal percentage was 98.2% by Fe_3O_4@Ag/SiO_2 even at the minimum contact time of 10 min. This immediate uptake of ions may be attributed to only adsorbate and adsorbent interactions. There is negligible interference of solute-solute or solvent-solvent interactions. Similar trends were reported for MB removal by

using montmorillonite clay [16]. The percent dye removal was slightly decreased with increase in MB concentration. The removal efficacy was 98.9% for 10mg/50mL while it was for 99.3% 50mg/50mL. It may be attributed to occupation of binding sites on the Fe_3O_4@Ag/SiO_2 surface. However dissimilar results were obtained in the case of adsorption capacity. The adsorption capacity increased from 3.3 mg/g to 82.6 mg/g, as the initial MB concentration increased from 10 mg/g to 50mg/g. These results suggested that the actual amount of dye adsorbed per unit mass of the adsorbent increased with dye concentration. Garg et al observed similar trends for the removal of basic dyes from aqueous solution [19].

3.2.4 Effect of temperature

The effect of temperature on the adsorption behavior of MB was studied by varying temperature in the range of (10-50˚C). The results are presented in Fig 6b. It is evident from the figure that, the percent adsorption of MB increased from 92.0% to 98.8% with the enhancing temperature at equilibrium. It is may be due to increased mobility of ions increased with a rise in temperature. Hence provides a smoother way for the formation of the monolayer. Secondly, it may be attributed to diffusion of adsorbate molecules to the external boundary layer and internal pores of Fe_3O_4@Ag/SiO_2.These results having resemblance with the findings of other investigators for the adsorption of MB [17].

3.3 Equilibrium isotherms

The equilibrium isotherm models play an important role in describing interactive behaviour between adsorbent and adsorbate molecules. Langmuir and Freundlich models were studied for the current equilibrium data of MB removal.

Langmuir Isotherm Model

The Langmuir equilibrium isotherm model assumes monolayer distribution of dye at specific homogeneous sites within the adsorbent surface and no interaction between

adsorbed species. A linearized form of Langmuir model is represented by the equation given below; [20]

$$\frac{C_e}{q_e} = \frac{1}{q_{max}b} + \frac{C_e}{q_{max}} \quad (3)$$

where q_{max} (mg/g) is the maximum adsorption capacity at monolayer coverage, *b* (L/mg) is the Langmuir constant parameter related to the energy of adsorption and affinity of binding sites between adsorbate and adsorbent. The plot of C_e/q_e vs $C_e$was found to be linear (Fig. 7a). The value of q_{max} (mg/g), *b* (L/mg) and correlation coefficient (R^2) was determined from plot of C_e/q_e vs C_e and given in Table 2.

Freundlich Isotherm Model

Freundlich isotherm model is applicable for the heterogenous surface system. A linear form is represented as [21].

$$logq_e = logK_f + \frac{1}{n} logC_e \quad (4)$$

where K_f is Freundlich constant which is related to the capacity of adsorbent for the adsorbate and 1/*n* is the heterogeneity factor related to the intensity of adsorption. A linear regression plot between log q_e and log C_e determines the values of K_f, *n* and correlation coefficient (R^2) (Fig. 7b). The values of *n* should lie in between 1 to 10 for favourable adsorption [30]. The values of adsorption parameters are given in Table 2.

The R^2 (0.971) value for Langmuir isotherm is greater than the R^2 (0.910) value for Freundlich isotherm. This confirms that the adsorption equilibrium of MB onto Fe_3O_4@Ag/SiO_2 explains better by the former than the later. The maximum monolayer adsorption capacity calculated by Langmuir isotherm was 128.45 mg/g which was comparable to the other adsorbents used in recent years for the removal of MB from the aqueous systems (Table 5).

3.4Adsorption Kinetics

In order to evaluate the rate mechanism of the adsorption of MB, pseudo-first order (Langergren rate eq.), pseudo-second order equation and intraparticle diffusion equation were applied to the experimental kinetic data. Langergren-first-order equation [22], pseudo-second-order equation [23] is represented as;

$$\log(q_e - q_t) = log q_e - \left(\frac{k_1}{2.303}\right) t \quad (5)$$

$$\frac{t}{q_t} = \frac{1}{k_2\, q_e^2} + \frac{t}{q_e} \quad (6)$$

where q_e and q_t (mg/g) are the amount of dye adsorbed per unit mass of the adsorbent at any time t and equilibrium time, respectively, and k_1 is pseudo-first order kinetic rate constant, k_2 is the equilibrium rate constant of the pseudo-second order equation The values of k_1 (min^{-1}) and q_e were calculated from a linear plot between log ($q_e - q_t$) and t at different concentration of MB (Fig. 8ab).

The plot between t/q versus t shows the pseudo second order model and ln(qe_qt) versus t shows the pseudo first order model (Fig. 8ab), respectively. At all concentration of MB, lower regression coefficient R^2 (0.7861-0.928) and large deviation between experimental and theoretical values of adsorption capacity were obtained for pseudo first order model. It confirms the nonapplicability of pseudo first order model to the experimental kinetic data. However, the higher correlation coefficient R^2 =0.999 was obtained from the pseudo second order model at all the concentration of MB in addition with negligible difference in qe experimental (82.3-16.3 mg/g) to theoretical (81.9-16.6 mg/g) [Table3]. These results demonstrate were well fitted to the pseudo second order model to interpret experimental kinetic data.

Intraparticle Diffusion is represented by following equation [24];

$$q_t = k_{id} t^{1/2} + C \quad (6)$$

where k_{id} is the intraparticle diffusion rate constant. C is intercept which provides an approximation about the thickness of the boundary layer. The value of k_{id} and C were calculated from the plot between $t^{1/2}$versus q_t shown in Fig. 8c. As seen in Fig, plot of uptake is linear, which confirms intraparticle diffusion process involved in the adsorption kinetics of MB but these lines did not pass through the origin. It confirms not only intraparticle diffusion is a rate controlling step, but also other kinetic models also involved in the adsorption process. The calculated correlation coefficient for all the concentration of MB was ($R^2 \geq 0.905$). According to the above discussion, adsorption of MB is a complex diffusion process consisting of boundary layer effect. Similar findings were observed by Nagarethinam et al [22]. The values of all kinetic parameters are given in Table 3.

3.5 Thermodynamic parameters

Adsorption of MB was studied in the temperature ranges (10 - 50 ˚C) keeping all the parameters constant to elaborate the thermodynamic parameters at equilibrium. Enthalpy (ΔH^0), Entropy (ΔS^0) and Gibb's free energy (ΔG^0) are related to the adsorption thermodynamic parameters. All of these were calculated by using the following equations [25]:

$$\Delta G^0 = -RTlnK_d \quad (7)$$

$$K_d = \frac{C_m}{C_e} \quad (8)$$

$$\Delta G^0 = \Delta H^0 - T\Delta S^0 \quad (9)$$

where ΔG^0 (kJ mol^{-1}), ΔH^0 (kJ mol^{-1}) and ΔS^0 (J $mol^{-1}K^{-1}$) are changes of Gibbs free energy, enthalpy and entropy, respectively. R is the universal gas constant (8.314 J $mol^{-1}K^{-1}$) and K_d is the equilibrium constant, C_m (mg/L) is the amount of dye on the adsorbent. The values of (ΔH^0), (ΔS^0) and $\Delta G^0$are calculated from the slope and intercept of the plot between $\ln K_d$ versus 1/T (Table 4). The negative value of ΔG^0 (-18.99 to -28.10 kJ mol^{-1}) at all the temperature and positive value of ΔS^0(228.3 J $mol^{-1}K^{-1}$) corresponds to the feasibility and spontaneity of the adsorption process. The adsorption

of Methylene Blue increases with increasing temperature. However, positive value of ΔH^0 (45.54 kJ mol^{-1}) implies the endothermic nature of the adsorption process [2, 3].

Mechanism of adsorption and role of Silver

Intermolecular forces were assumed between nanospheres and MB dye molecules. Ag nanoparticles covered the silica surface as Ag^+ ions. This surface covering of silver nanoparticles enhanced the catalytic reduction of dyes. Silver nanoparticles play the role of a catalyst for the reduction of dyes. These catalytic properties of silver towards reduction of dyes were observed by [26, 27]. The catalytic process can be explained by an electrochemical mechanism, where silver nanoparticles-supported silica spheres. Further, these silver supported silica shells complexed with Fe_3O_4 nanospheres. The iron oxide surface has a strong chemical affinity towards silica. No primer is required for deposition of silica on Fe_3O_4 nanospheres [28]. Polymeric chains of silica hydrogel produce three dimensional network of -$Si(OH)_2$-O-$Si(OH)_2$- groups onto silica water interface. That three dimensional network of -$Si(OH)_2$-O-$Si(OH)_2$ is hydrophilic and capable of holding a large number of [O^-] sites. Colloidal interactions of silica hydrogel are primarily strong vander wall interactions with the adsorbate surface [29]. The surface charge of nanospheres is highly negative. Hence there are electrostatic interactions and hydrogen bonding occurred among cationic MB dye molecules and negatively charged nanospheres. The mechanism of MB adsorption is shown in scheme 1.

Desorption studies

Regeneration of adsorbent is the key factor for economic treatment plants. Adsorbed methylene blue recovered from dye laden Fe_3O_4@Ag/SiO_2 nanspheres using hydrochloric acid of various strengths ranging from 0.1 to 0.3 M. 0.03 g of dye amalgamated Fe_3O_4@Ag/SiO_2 were added to 15 ml of HCl of desired concentration and agitated for 60 minutes in a closed shaker. As the results depicted in Fig 9a. desorption efficiency was increased from 44.3% to 77.5% with increasing HCl concentration.

However an optimum was observed at 0.025M, further on desorption efficiency remained constant. At lower pH, H^+ sites increased which favours the regeneration of MB.

Reuse of Fe_3O_4@Ag/SiO_2 nanospheres

Six adsorption-desorption cycles are repeated to recognize the reuse potential of Fe_3O_4@Ag/SiO_2 nanspheres. Fe_3O_4@Ag/SiO_2 nanspheres retain high removal efficiency (80.16-87.62%) during three consecutive cycles. Then kept constant at (~65.9%) for further three cycles as shown in Fig. 9b. That measure significant high adsorption efficiency of Fe_3O_4@Ag/SiO_2 nanospheres for several cycles.

4 Conclusion

In summary, silver silica coated magnetite (Fe_3O_4@Ag/SiO_2) nanospheres have been synthesized using sonication technique for efficient removal of Methylene Blue. Adsorption process was affected by pH, time, initial dye concentration and adsorbent dose. Equilibrium Isotherm modeling revealed that the experimental data fitted well with the Langmuir isotherm as compared to Freundlich Isotherm. Maximum adsorption capacity was 158.45 mg/g for 0.01g/50mL dye system. Kinetic data well fitted with the pseudo-second order and intraparticle diffusion model kinetics. The calculated values of thermodynamic parameters support spontaneous and endothermic nature of the adsorption process. The results demonstrated (99.8%) removal of MB. The adsorbent was regenerated and reusable through several cycles successfully. Fe_3O_4@Ag/SiO_2 could be a potential adsorbent for waste water treatment due to its high adsorption capacity.

References

1. J. Saini, V. K. Garg, R. K. Gupta, N. Kataria, Removal of Orange G and Rhodamine B dyes from aqueous system using hydrothermally synthesized zinc oxide loaded activated carbon (ZnO-AC), J. Environ. Chem. Engineering. 5 5420 (2017)
2. N. Kataria and V. K. Garg, Removal of Congo red and Brilliant green dyes from aqueous solution using flower shaped ZnO nanoparticles, J. Environ. Chem. Engineering. 5 5420 (2017)

3. U. Pal, A. Sandoval, S. I. U. Madrid, G. Corro,V. Sharma, P. Mohanty, Mixed titanium, silicon, and aluminum oxide nanostructures as noveladsorbent for removal of rhodamine 6G and methylene blue as cationic dyes from aqueous solution, Chemosphere. 163 (2016) 142-152
4. C. Hui, C. Shen, J. Tian, L. Bao, H. Ding, C. Li, Y. Tian, X. Z. Shiab H, J. Gao, Core-shell Fe_3O_4@SiO_2 nanoparticles synthesized with well-dispersed hydrophilic Fe_3O_4 seeds, Nanoscale. 3 (2011) 701–705
5. A. Morel, S. I. Nikitenko, K. Gionnet, A. Wattiaux, J. Lai-Kee-Him,C. Labrugere, B. Chevalier, G. Deleris, C. Petibois, A. Brisson, M. Simonoff, Sonochemical Approach to the Synthesis of Fe_3O_4@SiO_2 Core Shell Nanoparticles with Tunable Properties, ACS Nano. 5 (2008) 847–856
6. H. L. Ding, Y. X. Zhang, S. Wang, J. M. Xu, S. C. Xu, and G. H. Li, Fe_3O_4@SiO_2 Core/Shell Nanoparticles: The Silica Coating Regulations with a Single Core for Different Core Sizes and Shell, Chem. Mater. 24 (2012) 4572−4580
7. Y. Zhao, J. Li, L. Zhao, S. Zhang, Y. Huang, X. Wua, X. Wanga, Synthesis of amidoxime-functionalized Fe_3O_4@SiO_2 core–shell magnetic microspheres for highly efficient sorption of U(VI), Chem. Eng. J. 235 (2014) 275–283
8. L. Sun, S. Hu, H. Sun, H. Guo, H. Zhu, M. Liu, H. Sun, Malachite green Adsorption onto Fe_3O_4@SiO_2-NH_2:Isotherms, Kinetic and Process Optimization, RSC Adv. 5 (2015) 11837–11844
9. E. K. Pasandideh, B. Kakavandi, S. Nasseri1, A. H. Mahvi1, R. Nabizadeh, Silica-coated magnetite nanoparticles coreshell spheres (Fe_3O_4@SiO_2) for natural organic matter removal, J. Environ. Health Sci. Eng. 5 (2016) 14-21
10. L. Shi, L. Hu, J. Zheng, M. Zhang, J. Xu, Adsorptive Removal of Methylene Blue from Aqueous Solution using a Ni-Metal Organic Framework Material, J. Disper. Sci and Technol. 37(2016)1226-1231
11. W. Xiang-Feng, Z. Jie, S. Yang, D. Nai-Fu, Y. Xiao-Ying, Z. Ze-Huav, Solvothermal Preparation of Zinc Oxide/Reduced Graphene Oxide Composites for Rapid Removal of Methylene Blue, J. Nanosci. Nanotechnol. 17 (2017) 517-523

12. T. N. Hai, Comments on "Effect of Temperature on the Adsorption of Methylene Blue Dye onto Sulfuric Acid–Treated Orange Peel", J. Chem. Eng. Commun. 204 (2017) 134–139
13. M. T. Uddin, M. A. Islam, S. Mahmud, M. Rukanuzzaman, Adsorptive removal of methylene blue by tea waste, J. Hazard. Maters. 164 (2009) 53–60
14. F. A. Pavan, A. C. Mazzocato, Y. Gushikem, Removal of methylene blue dye from aqueous solutions by adsorption using yellow passion fruit peel as adsorbent, Bioresour. Technol. 99 (2008) 3162–3165
15. C.A.P. Almeida, N.A. Debacher, A. J. Downsc, Removal of methylene blue from colored effluents by adsorption on montmorillonite clay, J. Colloid Interface Sci. 332 (2009) 46–53.
16. M. A. Rahman, S. M. R. Amin, A. M. S. Alam, Removal of Methylene Blue from Waste Water Using Activated Carbon Prepared from Rice Husk, Dhaka University Journal of Science 60 (2012) 185-189
17. S. Patil, S. Renukdas, N. Patel, Removal of methylene blue, a basic dye from aqueous solutions by adsorption using teak tree (Tectona grandis) bark powder, Int. J. Environ. Sci. 1 (2011) 711-725
18. V.K. Garg, M. Amita, R. Kumar, R. Gupta, Basic dye (methylene blue) removal from simulated wastewater by adsorption using Indian Rosewood sawdust: a timber industry waste, Dyes Pigms.63 (2004) 243-250
19. N. Kannan, M. M. Sundaram, Kinetics and mechanism of removal of methylene blue by adsorption on various carbons—a comparative study Dyes Pigms. 51 (2001) 25–40
20. I. Langmuir, The adsorption of gases on plane surfaces of glass, mica and platinum, J. Am. Chem. Soc.40 (1918**)** 1361–1403.
21. H. Freundlich, Uber die adsorption in lasugen, J. Phys. Chem. 57 (1906) 385–470.
22. S. Lagergren, About the theory of so-called absorption of soluble substances Kungliga Svenska Vetenskapsakademiens Handlingar 24 (1898) 1–3.

23. Y. S. Ho, G. Mckay, Pseudo-second order model for sorption processes, Biochem. 34 (1999) 451–465.
24. W. Weber, J. Morris, Kinetics of adsorption on carbon from solution, J. Sanit. Eng. Div. 89 (1963) 31–60.
25. J. M. Smith, H. C. Ness, Introduction to Chemical Engineering Thermodynamics, McGraw-Hill New York, USA, 1987.
26. Z. Deng, M. Chen, L. Wu, Novel Method to Fabricate SiO_2/Ag Composite Spheres and Their Catalytic Surface-Enhanced Raman Scattering Properties, J. Phys. Chem. C. 111 (2007) 11692-11698.
27. Z. J. Jiang, C. Y. Liu, L. W. Sun, Catalytic Properties of Silver Nanoparticles Supported on Silica Spheres, J. Phys. Chem. C. 109 (2005) 1730-1735
28. Y. Lu, Y. Yin, B. T. Mayers, Y. Xia Modifying the Surface, Superparamagnetic Iron Oxide Nanoparticles through A Sol-Gel Approach, Nano Lett. 2 (2002) 183-186.
29. G. Vigil, Z. Xu, S. Steinberg, J. Israelachvili, Interactions of Silica Surfaces, J. Colloid Interface Sc. 165 (1994) 367-385
30. C. Dura, D. Ozdes, A. Gundogdu, H. B. Senturk, Kinetics and Isotherm Analysis of Basic Dyes Adsorption onto Almond Shell (Prunus dulcis) as a Low Cost Adsorbent, J. Chem. Eng. Data 56 (2011) 2136–2147
31. W. Zhang, C. Zhou, W. Zhou, A. Lei, Q. Zhang, Q. Wan, B. Zou, Fast and Considerable Adsorption of Methylene Blue Dye onto Graphene Oxide, Bulletin of Environmental Contam. Toxicol. (2011) 87:86–90
32. A. K. Nayak, A. Pal, Green and efficient biosorptive removal of methylene blue by Abelmoschus esculentus seed: Process optimization and multi-variate Modeling, J. Environ. Manage. 200 (2017) 145-159
33. P. Wang, M. Cao, C. Wang, Y. Ao, J. Hou, J. Qian, Kinetics and thermodynamics of adsorption of methylene blue by a magnetic graphene-carbon nanotube composite, Appl. Surf. Sci. 290 (2014) 116– 124

34. N. Gupta, A. K. Kushwaha, M. C. Chattopadhyaya, Application of potato (Solanum tuberosum) plant wastes for the removal of methylene blue and malachite green dye from aqueous solution, Arab. J. Chem. 1 (2016) 707-716

35. H. Mazaheri, M. Ghaedi, S. Hajati, K. Dashtian, M. K. Purkait, Simultaneous removal of Methylene blue and Pb^{2+} ion using Ruthenium nanoparticle-loaded activated carbon; Response surface methodology, RSC Adv. 5 (2015) 83427-83435

36. S. Y. Mak, D. H. Chen, Fast adsorption of methylene blue on polyacrylic acid-bound iron oxide magnetic nanoparticles, Dyes Pigms. 61 (2004) 93–98

37. W. Wang, Z. Ding, M. Cai, H. Jian, Z. Zeng, F. Li, J. P. Liu, Synthesis and high-efficiency methylene blue adsorption of magnetic PAA/$MnFe_2O_4$ nanocomposites, Appl. Surf. Sci. 346 (2015) 348–353

38. W. Wang, Kai Cai, X. Wu, X. Shao, X. Yang, A novel poly(m-phenylenediamine)/reduced graphene oxide/nickel ferrite magnetic adsorbent with excellent removal ability of dyes and dyes and Cr (VI), J. Alloys. Compd. 722 (2017) 532-543

39. K. Cai, W. Shen, B. Ren, J. He, S. Wu, W. Wang, A phytic acid modified $CoFe_2O_4$ magnetic adsorbent with controllable morphology, e excellent selective adsorption for dyes and ultra-strong adsorption ability for metal ions, J. Chem. Eng. 330 (2017) 936-946

40. D. Das, P. Choudhury, L. Bortahkur, B. Gogoi, A. K. Buragohai, S. K. Dolui, Synthesis and characterization of SiO2/polyaniline/Ag core–shell particles and studies of their electrical and hemolytic properties: multifunctional core–shell particles, RSC Adv. 5 (2015) 2360-2367

Caption of figures

Figure 1 (a-c) FT-IR spectrum Fe_3O_4, Ag/SiO_2 and $Fe_3O_4@Ag/SiO_2$ nanospheres.

Figure 2 (a-c) XRD patterns of Fe_3O_4, Ag/SiO_2 and $Fe_3O_4@Ag/SiO_2$nanospheres.

Figure 3 (a-d) SEM images of Fe_3O_4, Ag/SiO_2 and $Fe_3O_4@Ag/SiO_2$ of nanospheres.

Figure 4 a-d) TEM images of $Fe_3O_4@Ag/SiO_2$ nanospheres e) EDX of $Fe_3O_4@Ag/SiO_2$nanospheres.

Figure 5 (a) Effect of pH on adsorption of MB on $Fe_3O_4@Ag/SiO_2$ nanospheres. (Experimental Conditions: dye conc.-50 mg/L, dose - 0.03g/50mL, temp. - 27˚C, contact time – 50 min.) (b) Effect of Adsorbent Dose on adsorption of MB on $Fe_3O_4@Ag/SiO_2$ nanoparticles. (Experimental Conditions: pH – 7, dye conc.-50 mg/L, contact time – 50 min. , temp. - 27˚C)

Figure 6 (a) Effect of contact time with dye concentration on adsorption of MB dye on $Fe_3O_4@Ag/SiO_2$ nanospheres.. (Experimental Conditions: pH – 7, dye conc.- 10-50 mg/L, dose - 0.03g/50mL, temp. - 27˚C) (b) Effect of temperature for adsorption of MB dye on $Fe_3O_4@Ag/SiO_2$ nanoparticles. (Experimental Conditions: pH – 7, dye conc.-50 mg/L, dose - 0.03g/50mL)

Figure 7 Adsorption isotherms plots for removal of MB dye on $Fe_3O_4@Ag/SiO_2$ nanospheres. (a) Langmuir isotherm plot (b) Freundlich isotherm plot

Figure 8 Kinetic plots for adsorption MB dye on $Fe_3O_4@Ag/SiO_2$nanospheres. (a) pseudo-first order plot (b) pseudo-second order plot (c) intraparticle diffusion plot

Figure 9 (a) Desorption studies of MB onto $Fe_3O_4@Ag/SiO_2$ nanospheres. (b) Removal efficiencies of MB onto $Fe_3O_4@Ag/SiO_2$ nanospheres during six adsorption– desorption cycles

Tables:

.

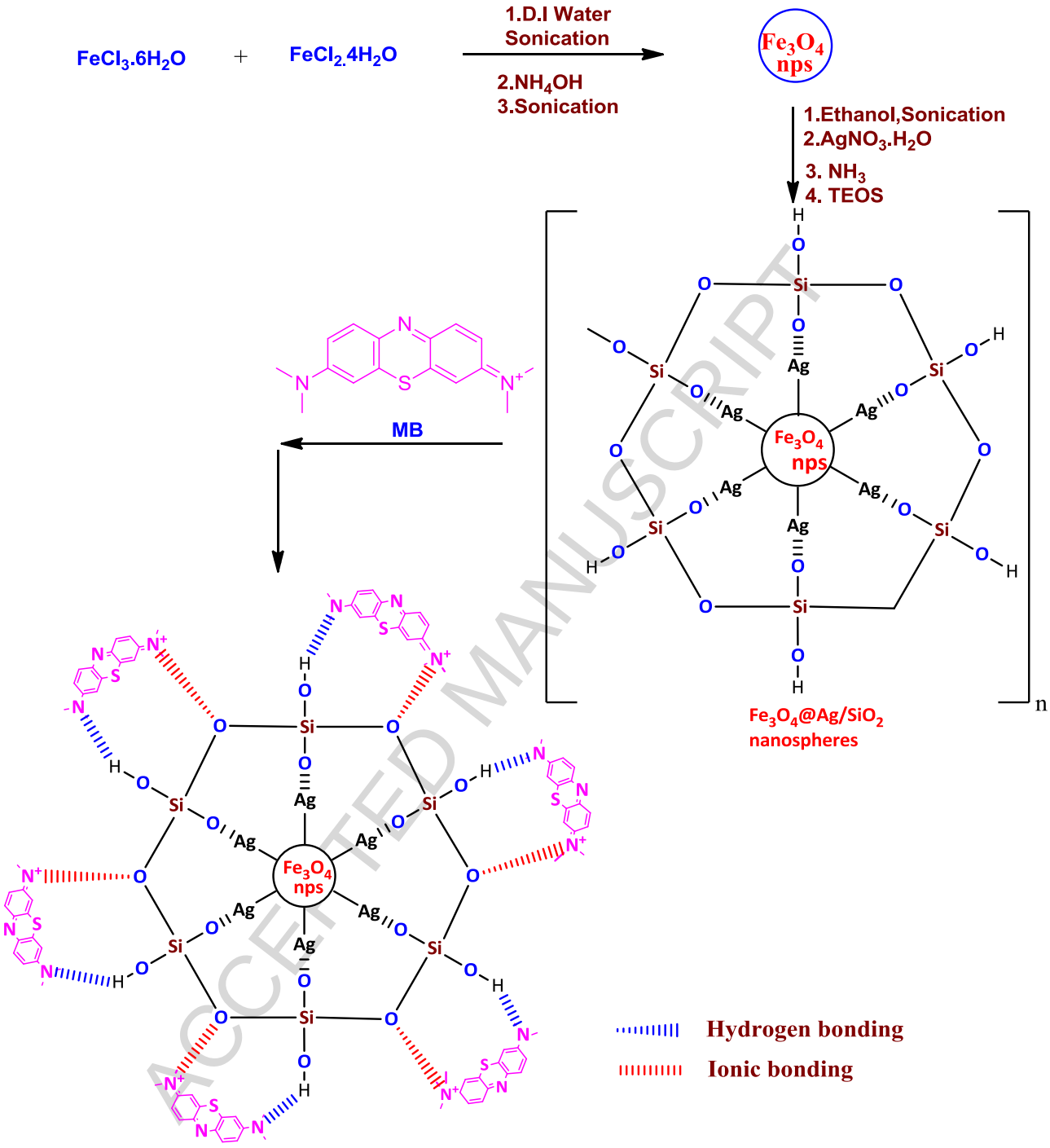

Scheme 1: Proposed mechanism for interactions of MB onto Fe_3O_4@Ag/SiO_2 nanoparticles

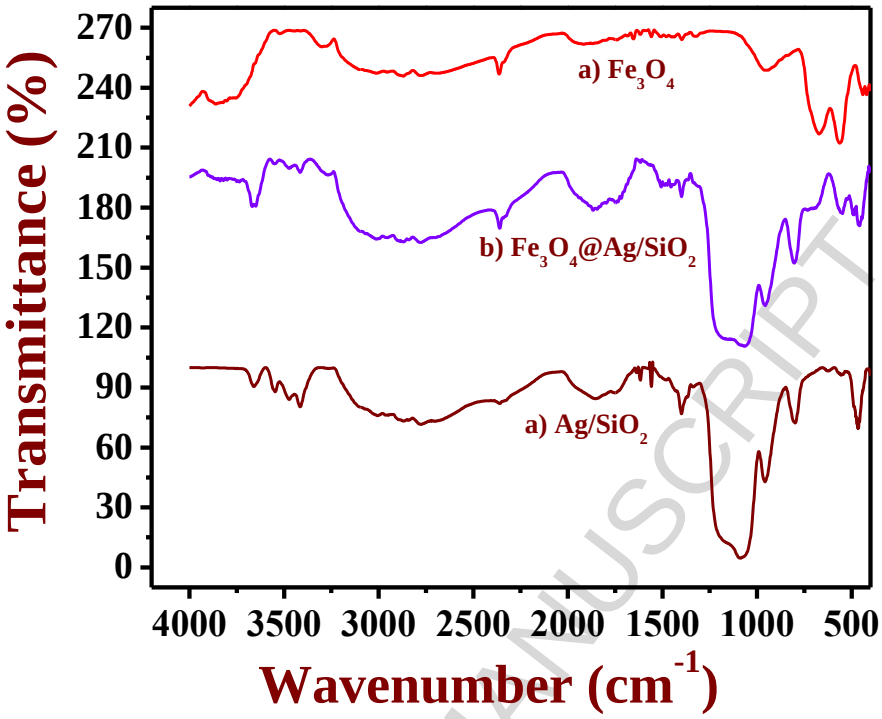

Figure 1(a-c) FT-IR spectrum of Fe_3O_4, Fe_3O_4@Ag/SiO_2, and Ag/SiO_2 nanospheres

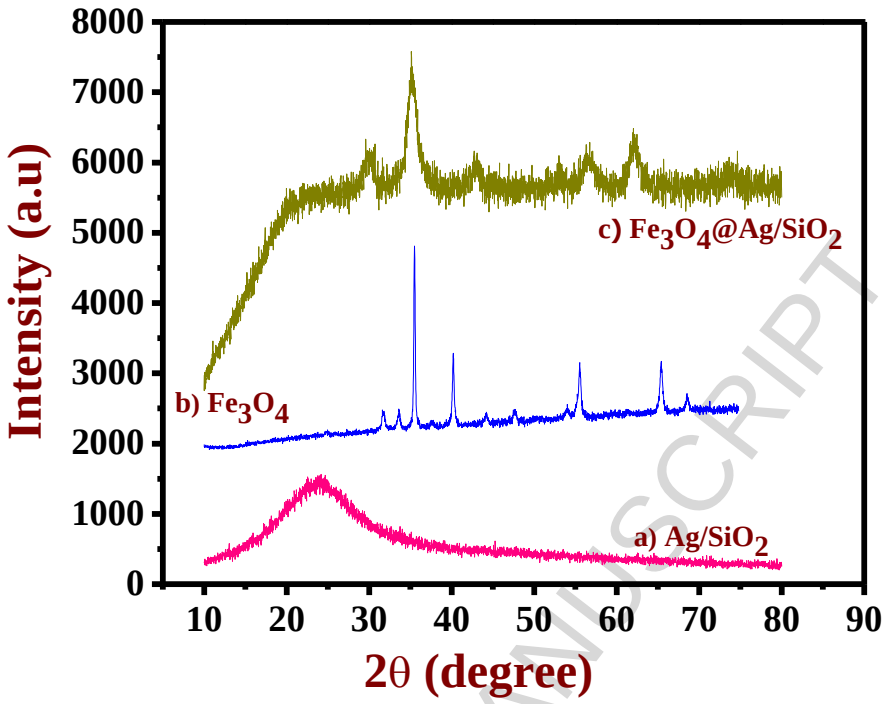

Figure 2(a-c) XRD patterns of Ag/SiO_2, Fe_3O_4 and $Fe_3O_4@Ag/SiO_2$ nanospheres

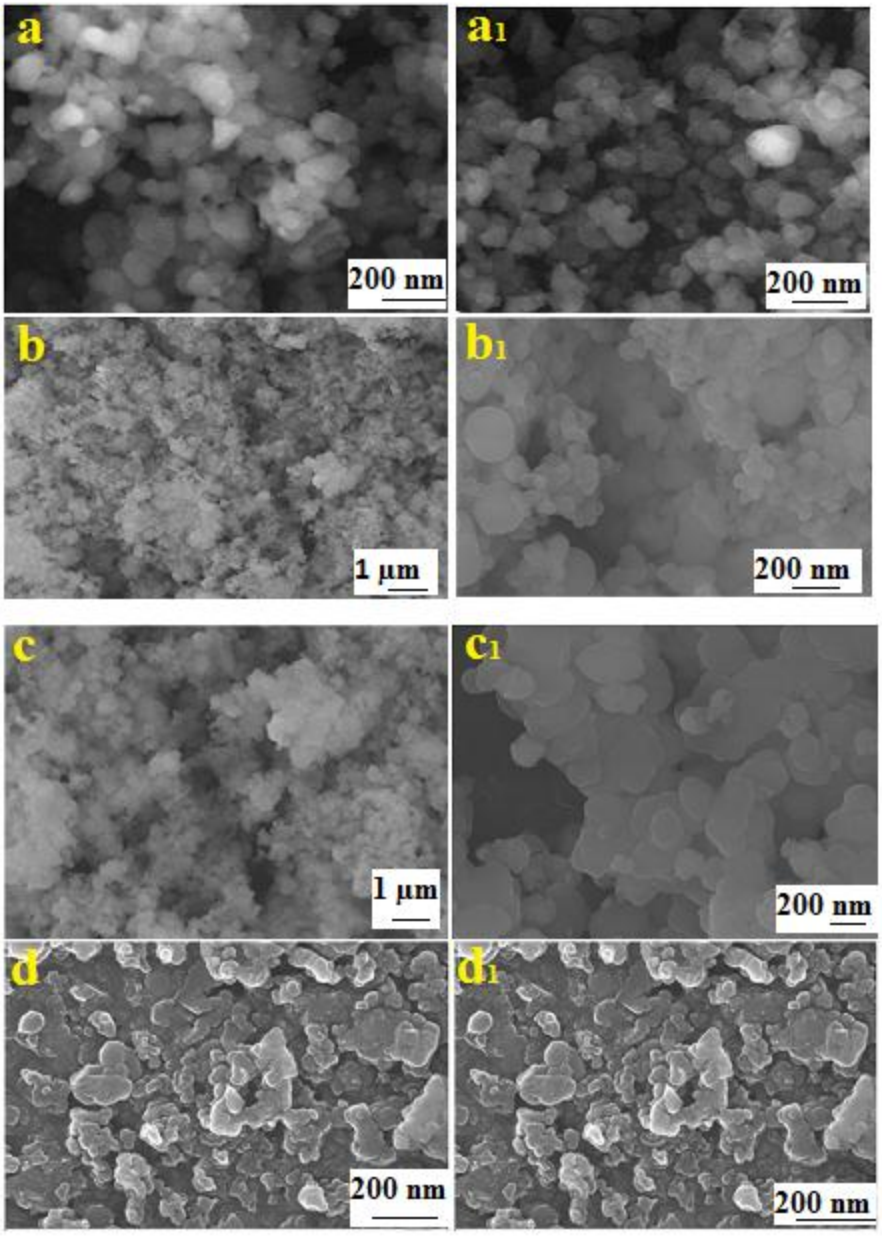

Figure 3(a-d) SEM images of**3aa$_1$.** Fe_3O_4, **3bb$_1$.** Ag/SiO_2 and **3cc$_1$**. Fe_3O_4@Ag/SiO_2nanospheres. **3dd$_1$.** SEM image of Fe_3O_4@Ag/SiO_2 nanospheres after adsorption

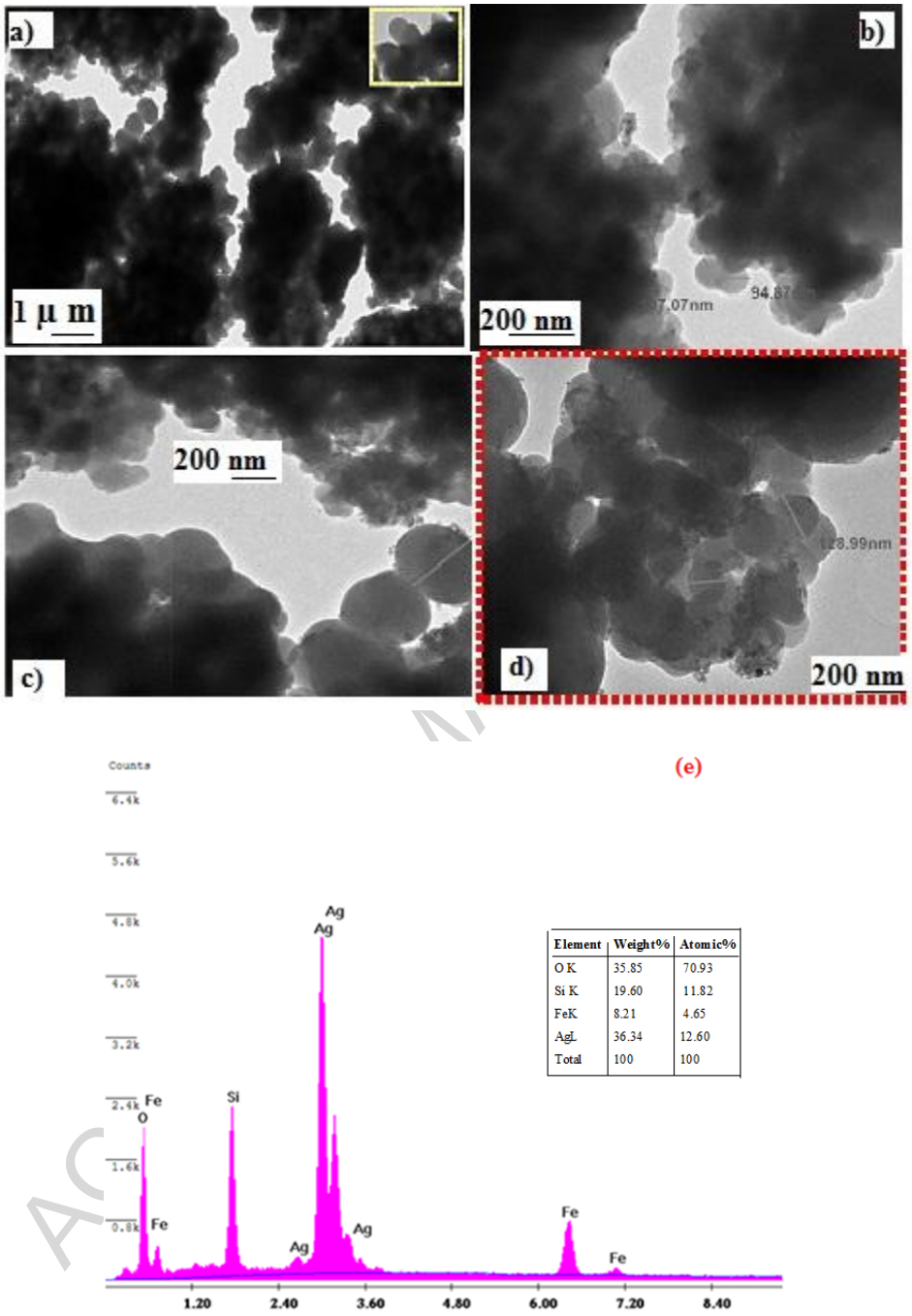

Figure 4. a-d) TEM images of Fe_3O_4@Ag/SiO_2 nanospheres e) EDX of Fe_3O_4@Ag/SiO_2 nanospheres

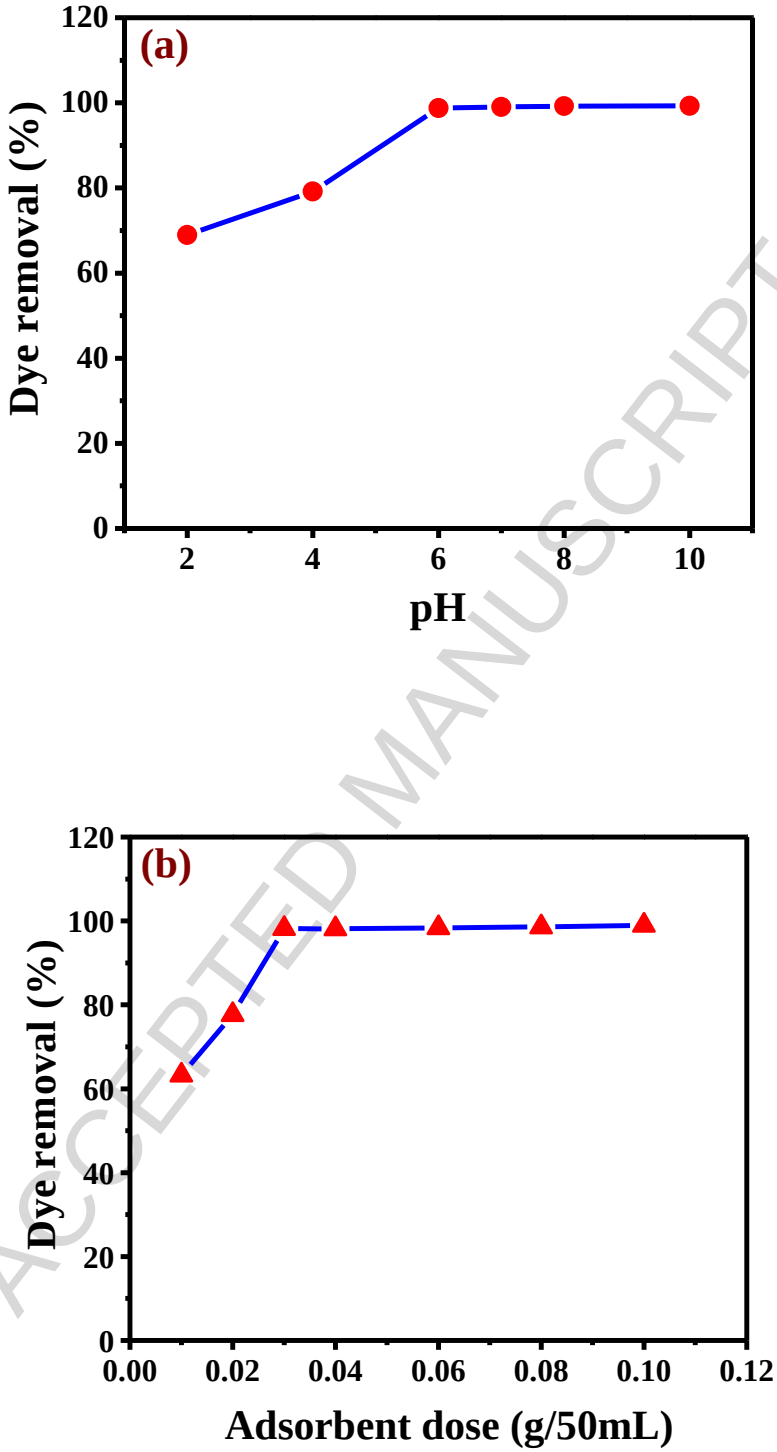

Figure 5 (a) Effect of pH on adsorption of MB on Fe_3O_4@Ag/SiO_2nanospheres. (Experimental Conditions: dye conc.-50 mg/L, dose - 0.03g/50mL, temp. - 27˚C, contact time – 50 min.) (b) Effect of Adsorbent Dose on adsorption of MB on Fe_3O_4@Ag/SiO_2 nanospheres.. (Experimental Conditions: pH – 7, dye conc.-50 mg/L, contact time – 50 min. , temp. - 27˚C)

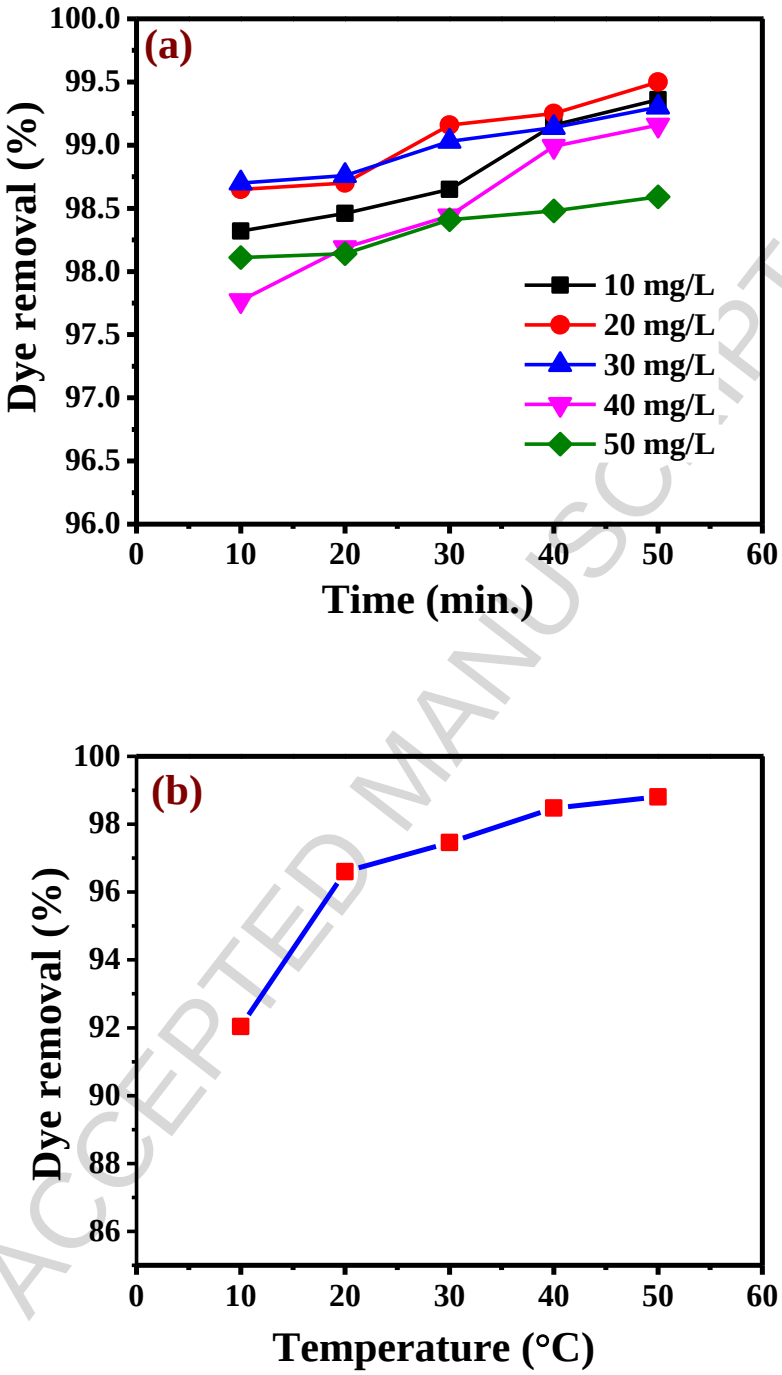

Figure 6 (a) Effect of contact time with dye concentration on adsorption of MB dye on Fe_3O_4@Ag/SiO_2nanospheres.. (Experimental Conditions: pH – 7, dye conc.- 10-50 mg/L, dose - 0.03g/50mL, temp. - 27˚C) (b) Effect of temperature for adsorption of MB dye on Fe_3O_4@Ag/SiO_2 nanospheres.. (Experimental Conditions: pH – 7, dye conc.-50 mg/L, dose - 0.03g/50mL)

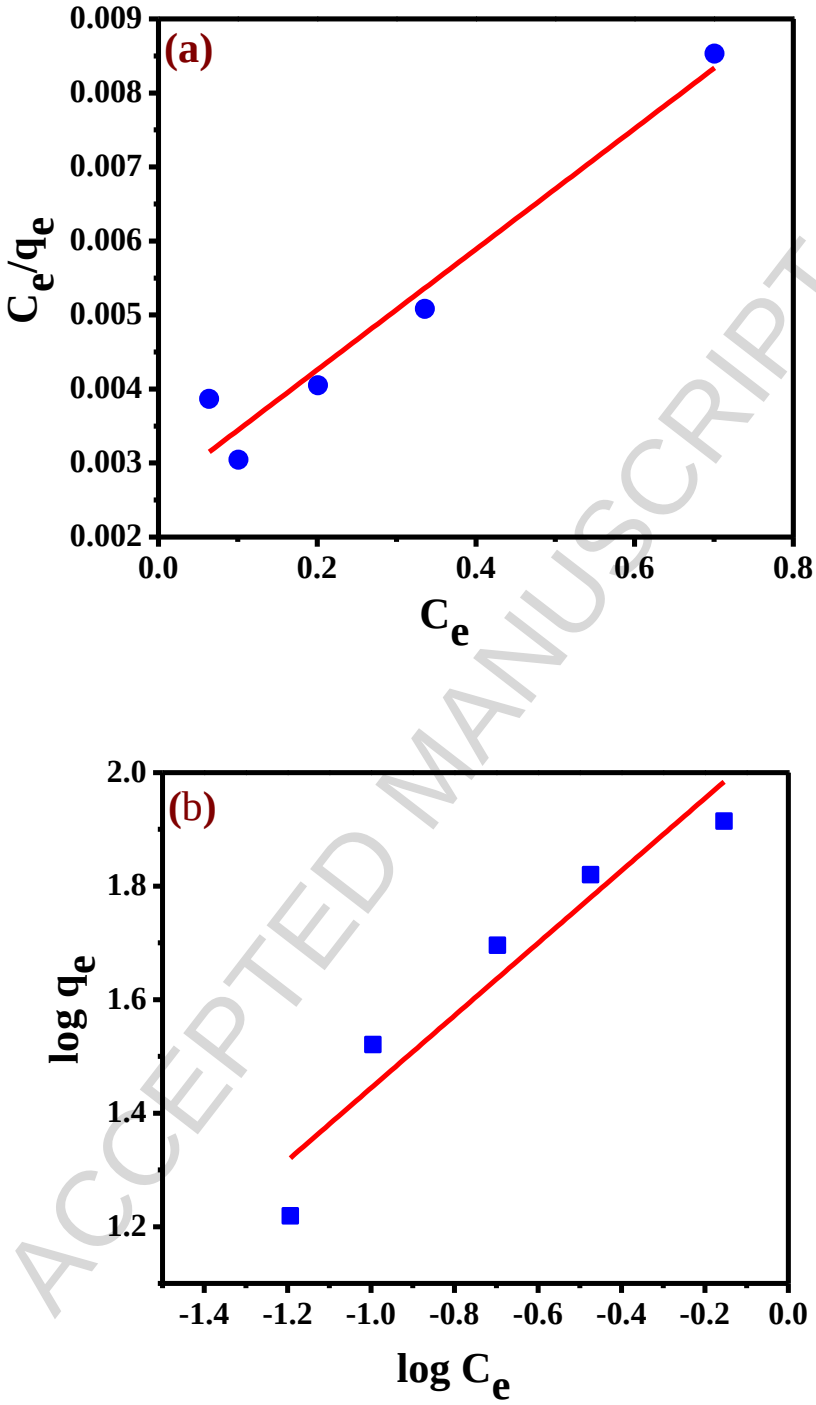

Figure 7 Adsorption isotherms plots for MB dye on Fe_3O_4@Ag/SiO_2 nanospheres. (a) Langmuir isotherm plot (b) Freundlich isotherm plot

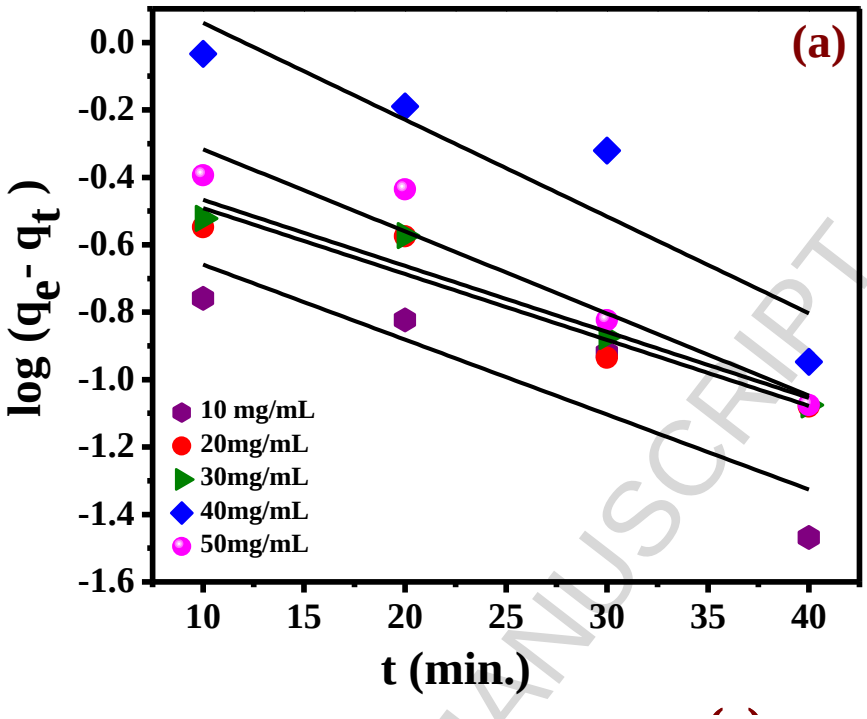

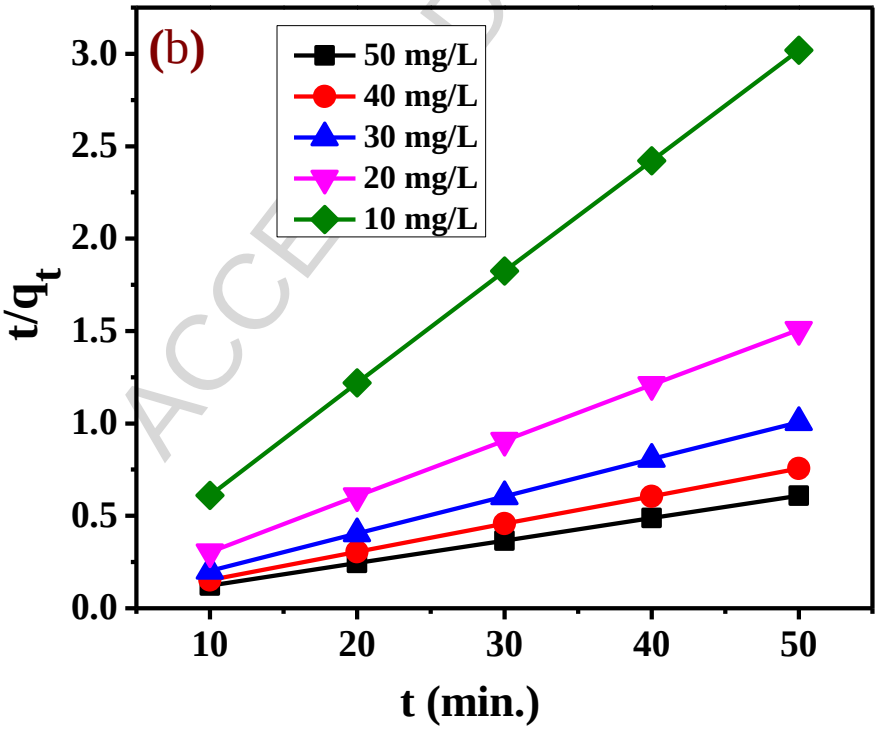

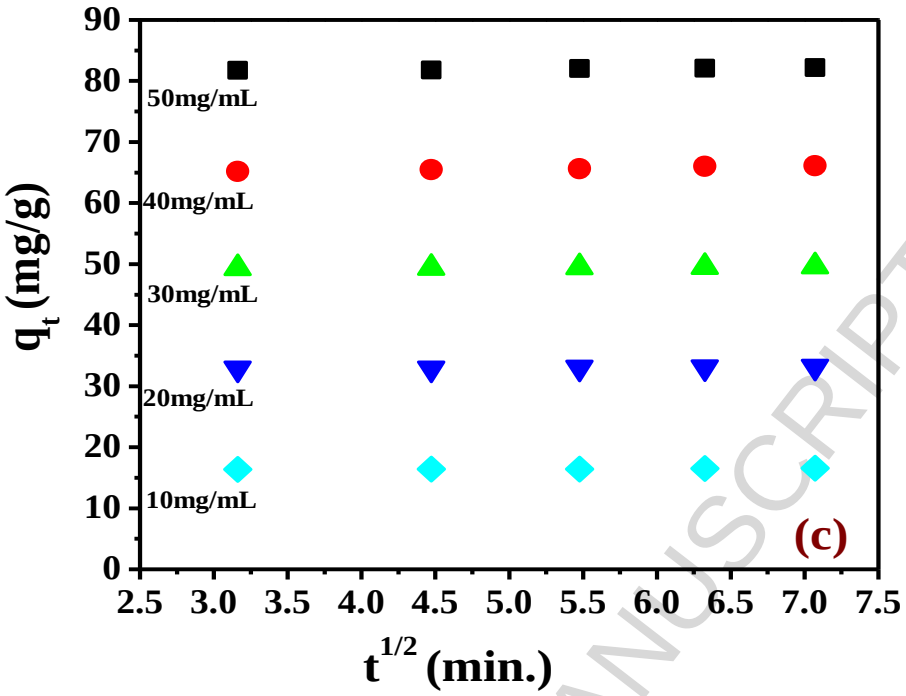

Figure 8 Kinetic plots for adsorption MB dye on Fe_3O_4@Ag/SiO_2 nanospheres. (a) pseudo-first order plot (b) pseudo-second order plot (c) intraparticle diffusion plot.

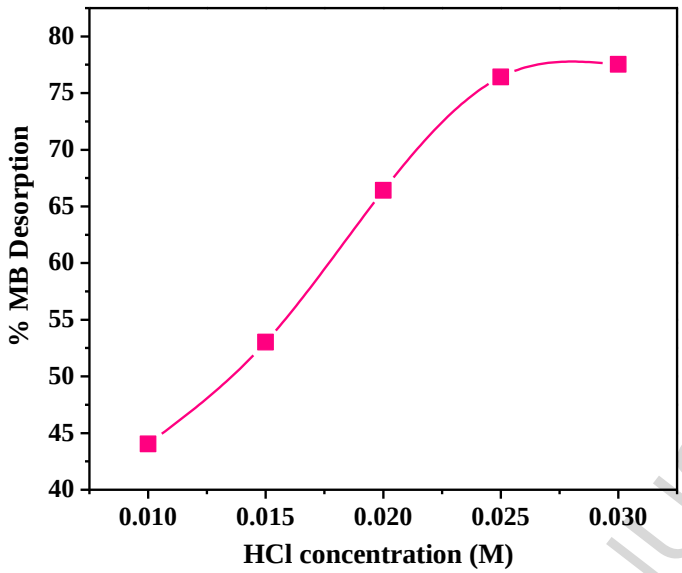

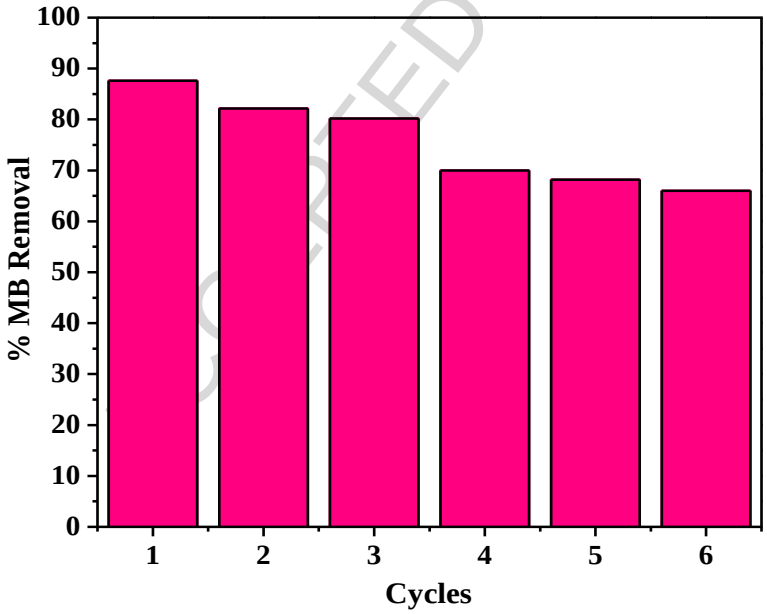

Fig 9 (a) Desorption studies of MB onto Fe_3O_4@Ag/SiO_2 nanospheres. (b) Removal efficiencies of MB onto Fe_3O_4@Ag/SiO_2 nanospheres during six adsorption– desorption cycles

Table 1. Properties and structure of Methylene Blue dye

Dye	Methylene Blue
Molecular formula	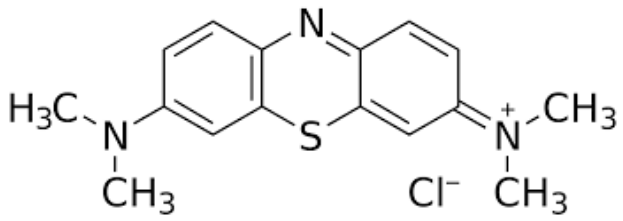
Molecular weight (g/mole) Classification C.I. no C.I. name Melting point (˚C) Dye content (%) λ_{max} (nm) Physical state	319.85 Basic dye 52015 Basic blue 9 190 95% 590 Dark blue to brown powder

Table 2.
Various adsorption isotherm models for MB dye adsorption interpreted by correlation coefficients and adsorption parameters

Isotherms model	Linear equation	Parameters	Values
Langmuir	$C_e/q_e = 1/q_{max}b + C_e/q_{max}$	q_{max}(mg/g)	128.45
		b(L/mg)	3.11
		R^2	0.967
Freundlich	$\log q_e = logK_f + 1/n\, logC_e$	n	1.567
		K_f(mg/g)	2.083
		R^2	0.915

Table 3 Kinetic models parameter study for MB dye adsorption on Fe_3O_4@Ag/SiO_2 nanospheres

Kinetic models	Parameters	Values of parameters				
		50 mg/l	40mg/l	30mg/l	20mg/l	10mg/l
Pseudo-first order	k_1 (min^{-1})	0.0559	0.0660	0.0451	0.0453	0.0511
	q_e(cal)	0.844	2.214	0.535	0.506	0.3660
	R^2	0.928	0.8579	0.942	0.911	0.7861
Pseudo-second order	k_2 (g/mg min)	0.1353	0.060	0.175	0.1887	0.283
	q_e (cal)	81.961	66.22	49.75	33.22	16.66
	R^2	0.999	0.999	0.999	0.999	0.999
Intraparticle diffusion	k_{id} (mg $g^{-1}min^{-1/2}$)	0.1115	0.2446	0.0796	0.0761	0.046
	CR^2	81.373	64.377	49.071	32.613	16.25
		0.938	0.976	0.951	0.924	0.905
Experimental data	q_e (exp)	82.16	66.10	49.65	33.16	16.33

Table 4 Thermodynamic parameters for MB dye adsorption over Fe_3O_4@Ag/SiO_2 nanospheres

T (K)	ΔG^{o} (k J mol^{-1})	ln(K_d)	ΔS^{0}(J $mol^{-1}K^{-1}$)	ΔH^{o} (k J mol^{-1})
283	-18.98	4.362	228.30	45.54
293	-21.26	4.408		
303	-23.54	4.417		
313	-25.83	4.427		
323	-28.12	4.431		

Table 5 Adsorption capacity of various adsorbents for MB

Adsorbent	**$q_{max.}$ (mg/g)**	**Reference**
Alomond shell (Prunus dulcis)	51.02	[30]
Mixed titanium, silicon, and aluminum oxide nanostructures	162.96	[3]
Graphene Oxide	19.39	[31]
Abelmoschus esculentus seed	205.65	[32]
Graphene-carbon multiwalled nanotube composites	65.79	[33]
Potato plant wastes (*Solanum tuberosum*)	52.6	[34]
Ruthenium nanoparticle loaded activated carbon (Ru-NPs-AC) nanocomposites	41.6	[35]
Rosewood sawdust	46.1	[18]
Polyacrylic acid-bound iron oxide magnetic nanoparticles	19.9	[36]
Montmorillonite clay	289.12	[15]
Yellow passion fruit peel	6.8	[14]
Tea waste	85.16	[13]
PAA/$MnFe_2O_4$ nanocomposite	53.3	[37]
Poly(phenylenediamine)/reduced graphene oxide/nickel ferrite magnetic adsorbent	37.0	[38]
Phytic acid modified $CoFe_2O_4$ magnetic adsorbent	54.8	[39]
Silver silica coated magnetite nanospheres (Fe_3O_4@Ag/SiO_2)	128.4	Present work

Highlights

- Fe_3O_4@Ag/SiO_2 nanospheres were synthesized via sonication technique.
- Excellent removal percentage of Methylene Blue (~100%) was achieved using Fe_3O_4@Ag/SiO_2 nanospheres.
- Possible electrostatic mechanism for dye removal was illustrated to understand the interactive behaviour of adsorbent and adsorbate.
- Fe_3O_4@Ag/SiO_2 nanospheres may be regenerated and reuse for several cycles.